Architectures of Translational Parallel Mechanism for MEMS Fabrication

Hagay Bamberger
RAFAEL-Advanced Defense Systems Ltd.,
Robotics Laboratory-Technion,
P.O. Box 5218,
Kfar Hasidim 20400, Israel
e-mail: hagayb@rafael.co.il

Alon Wolf
Mem. ASME
Biorobotics and Biomechanics Lab,
Technion,
Haifa 32000, Israel
e-mail: alonw@technion.ac.il

Moshe Shoham
Fellow ASME
Robotics Laboratory,
Technion,
Haifa 32000, Israel
e-mail: shoham@technion.ac.il

Manufacturing techniques, especially in the microscale, determine the type of joints, links, and actuators available for the designer, and as a result, the possible kinematic architectures of the designed mechanism. This paper discusses the design constraints imposed by current microelectromechanical system (MEMS) fabrication techniques, and how they affect the feasible kinematic architectures of microrobots. In particular, three degree-of-freedom translational mechanisms are investigated, and all possible nonoverconstrained kinematic architectures under limitations imposed by MEMS fabrication techniques are derived.
[DOI: 10.1115/1.2936933]

1 Introduction

Microelectromechanical system (MEMS) is a relatively new technology, enabling fabrication of miniature mechanical devices on silicon wafers. Most fabrication methods are based on lithography, which produces two-dimensional shapes by layer etching and deposition. Consequently, MEMS devices usually have a planar geometry, making it difficult to construct mechanisms that are fully three dimensional. The hinge design presented in Ref. [1] enabled, for the first time, the production of spatial mechanisms using surface micromachining. The hinge element is fabricated in the substrate plane, but it is free to rotate out of the plane. Connecting several of these hinges in a kinematical chain results in a structure that can be lifted off the plane, thus yielding a three-dimensional mechanism.

The components that constitute mechanisms are links, joints, and actuators. When dealing with microsystems, the fabrication techniques are of utmost importance for the mechanism designers since not all of the components can be realized by MEMS technology, which is the leading manufacturing technique for milimetric and submilimetric scale. Hence, manufacturing technology determines what types of links, joints, and actuators are at the designer disposal, which in turn affects the feasible kinematic architectures.

Universal joints and spherical joints, having two and three degrees of freedom (DOFs) respectively, are very rare and hard to manufacture using the current MEMS fabrication techniques. On the other hand, a simple revolute joint, whose axis is parallel to the substrate plane, is possible. This kind of joint enables a very large angle of revolution, even greater than 180 deg [1].

Electrostatic actuation [2] is a very common method, based on techniques derived from integrated circuit fabrication. Although a variety of geometries of electrostatic actuators have been developed, the linear design is the most commonly used, enabling relatively large displacements. This type of actuator can also be designed to enable bidirectional translation. Most actuators developed in MEMS are built on the silicon substrate and their stators are not raised above that plane. Therefore, it is preferable to use this common design to produce actuators that are linear and are located at the base of the mechanism. The architecture described in Ref. [3] is not suitable for MEMS fabrication, since the actuators do not lie in the same plane.

In Ref. [2], a translational three DOF MEMS mechanism was constructed using few simple revolute and compliant joints. The mechanism architecture is very simple, yielding simple inverse and direct kinematic solutions. One major advantage of this design is that the moving platform can be lifted off the plane by its own actuators. However, in order for the platform to have a reasonable workspace, the actuators need to have long stroke. Also, the compliant joints suffer from internal stresses that cause reaction forces applied on the actuators, even when the mechanism is in its natural position.

Another very important aspect of MEMS manufacturing is clearance at the joints, which are about only one order of magnitude less than the links themselves. This opens a whole new research field—large clearance mechanisms, which has been treated in a separate paper [4] and is omitted in the present discussion.

In this paper, we present a systematic way for designing architectures of large clearance mechanisms with applications to microparallel mechanisms. Our approach takes into account considerations related to MEMS fabrication limitations, as well as constraint singularities of limited DOF mechanisms. We denote this approach as *MEMS kinematics* since it comprises both MEMS constraints and fundamental kinematic rules in mechanism design. We start with a systematic search for a translational parallel mechanism that is suitable for MEMS fabrication techniques, i.e., consists of only revolute hinges, whose axes lie in the substrate plane during manufacturing, and linear actuators, which are located at the base. Then, we suggest two types of architectures, where one of them features topologically identical limbs. For those types, some kinematical analyses are presented, ending with numerical examples.

2 Possible Architectures of Three DOF Mechanisms

A *limited DOF parallel mechanism*, which is capable of less than six DOF, may suffer from *constraint singularity*, in which the platform gains extra uncontrollable motion [5–10]. When considering the singularity of a limited DOF mechanism, it is important to develop the full Jacobian matrix, which consists of two submatrices [5]: the Jacobian of actuations $\mathbf{J}_A$ and the Jacobian of constraints $\mathbf{J}_C$. This full Jacobian matrix is needed to determine the direct kinematic singularities, while another Jacobian matrix is helpful in detecting the inverse kinematic singularities, which are similar to those of a serial mechanism [11]. Reference [12] gives a comprehensive study to obtain all possible singularities, by considering all joint velocities, including the passive ones.

In a *nonredundant robotic mechanism*, the number of actuators is equal to the number of endeffector's DOF. When each limb

Contributed by the Mechanisms and Robotics Committee for publication in the JOURNAL OF MECHANICAL DESIGN. Manuscript received September 9, 2007; final manuscript received March 26, 2008; published online July 11, 2008. Review conducted by Larry L. Howell. Paper presented at the 12th World Congress in Mechanism and Machine Science (IftoMM) 2007.

Table 1 All combinations of nonredundant three DOF parallel mechanisms

	No. of links=No. of passive joints (n_l)			No. of constraints=No. of rows in $\mathbf{J}_C$		
Type	Limb 1	Limb 2	Limb 3	Limb 1	Limb 2	Limb 3
I	4	4	4	1	1	1
II	3	4	5	2	1	0
III	2	5	5	3	0	0

consists of one actuator at the base, this is the number of limbs that connect the base and the platform [13].

For trivial nongeometrically dependent joints, and not overconstrained mechanism, the mobility of a mechanism can be calculated by the well-known Grübler formula [14–16]:

$$M = \lambda(n - j - 1) + \sum_{i=1}^{j} f_i \tag{1}$$

where $\lambda=6$ for spatial mechanisms, n denotes the number of rigid bodies, j the number of joints (both active and passive), and f_i the number of DOF in each joint. Usually f_i equals 1 in MEMS, due to the manufacturing constraints. Denote n_l as the number of links in each of the three limbs, such that $n=2+\Sigma_{l=1}^{3} n_l$ and $j=\Sigma_{l=1}^{3}(n_l+1)$. Substituting $M=3$ for a three DOF mechanism yields $\Sigma_{l=1}^{3} n_l=12$. Each limb may consist of six joints at the most (i.e. $n_l \leqslant 5$), otherwise uncontrollable DOF occur in the serial part of the limb [17]. In light of that, the kinematical combinations in Table 1 are the only possible ones.

Consider now one limb of the mechanism. Each limb consists of one active joint, i.e., it contributes one row to the Jacobian of actuations, $\mathbf{J}_A$. This row is the screw that is reciprocal to all passive joints, but not to the active one in the limb [5]. The screw that is reciprocal to all the joints is a row in the Jacobian of constraints, $\mathbf{J}_C$. Such a screw cannot be found in a limb with five passive joints, since the connectivity of such a limb is six. However, in limbs that consist of four, three, or two passive joints, one can find one, two, or three reciprocal screws, respectively. Consequently, there are always three rows in the $\mathbf{J}_C$ matrix.

Indeed, the mobility formula [14] ensures that the number of DOF of the architectures specified in Table 1 is 3, but it does not provide any information on the nature of motion of the platform, whether it is rotational or translational. This paper focuses on pure translational mechanisms: therefore, all types given in Table 1 should be examined to verify if they can be considered as candidates for manufacture in MEMS; namely, they combine only revolute joints and linear actuators.

- Type I and Type II. These architectures can yield a translational only mechanism, as shown in the next sections of this paper.
- Type III. This type of architecture cannot yield a translational only mechanism, since Limb 1, which should prevent three rotational DOF, cannot accomplish that using its two revolute joints. Proof: If these joints are parallel to each other, they do not constrain the rotation about their common axis. In case that they are not parallel to each other, their angular velocities must be zero in order to satisfy the zero angular velocity of the platform [13,17].

3 Architecture of Type I

3.1 Options for Type I Architectures. For Type I architecture, the three limbs are topologically identical, consisting of a linear actuator, three links, and four passive joints. Each limb constraints the platform rotation about a single direction and hence contributes one row to $\mathbf{J}_C$. As has been proven in Ref. [13], in order to obtain a pure translational motion of the moving platform, the joints in each limb must be arranged as two pairs of parallel axes. In addition, due to the MEMS manufacturing processes, which enforce the joint axes to lie in the same plane, the two middle joint axes must intersect (i.e., skew axes are impossible).

A totally symmetrical architecture has been described by two of this paper's authors in Ref. [18]. This architecture was found to be in architectural singularity throughout its workspace, since the three limbs prevent platform rotation about the same direction, which is perpendicular to the base and the platform planes. Singularity of rank 2 of $\mathbf{J}_C$ results in two uncontrollable rotational DOFS of the platform. A slightly different architecture, which provides a solution to this constraint singularity problem, is given in Fig. 1 [19].

For this modified architecture, "one-time" revolute joints were introduced between the base and two of the actuators. These joints are manufactured as usual hinges, and are snapped and latched after being lifted off from the substrate plane. Consequently, each limb constrains the rotation about a different tilted direction, as indicated by the dashed lines in Fig. 1. Since the constraint vectors are no longer parallel, the mechanism is not singular and is capable of a pure translational motion. It is worth noting that the platform is parallel to the base, as in Ref. [18].

There is another way to overcome the constraint singularity problem, without adding one-time joints. The key to this solution lies in the different angles between the two pairs of parallel axes. These three angles determine the inclination of the platform after lifting it from the substrate plane. If these angles are different than 90 deg (Fig. 2), the platform inclines in a fixed orientation with respect to the base, and the mechanism is not singular. This kinematical architecture fits MEMS fabrication limitations, since it consists of revolute hinges only, whose axes lie in the substrate plane during the fabrication process, and linear actuators located at the base (Fig. 3).

3.2 Geometric Definitions for the Suggested Architecture. Perspective skeleton views, clarifying the subsequent definitions, are shown in Figs. 4 and 5.

A platform $P_{11}P_{21}P_{31}$ is connected to the base via three limbs. Each limb consists of three links, four revolute joints, and a linear actuator that is located at the substrate plane. The actuators determine the positions of points P_{i4} $(i=1,2,3)$. For simplicity, the

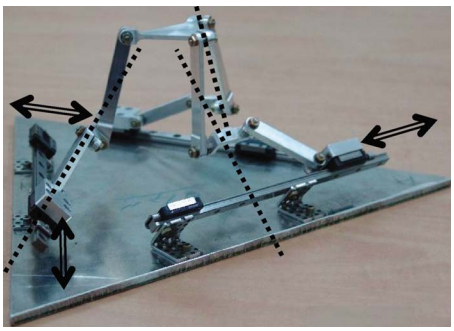

Fig. 1 Up-scale model of the nonsingular architecture, in which the platform is parallel to the base [19]. Each limb prevents platform rotation about its dashed line direction.

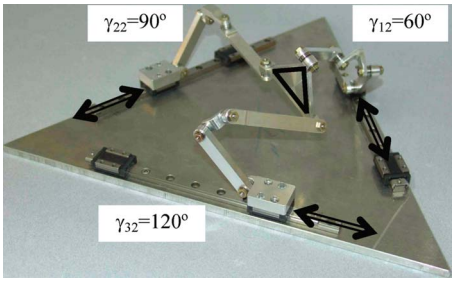

Fig. 2 Three DOF translational parallel mechanism

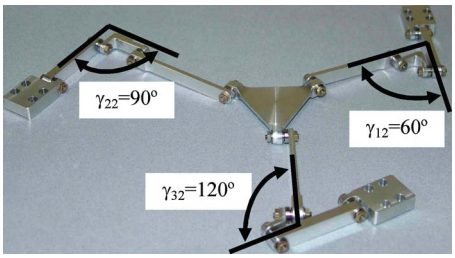

Fig. 3 Links and joints in a manufacturing configuration

passive joints at points P_{i4} are chosen to be perpendicular to the direction of motion of the actuator. According to the guidelines given in Ref. [13], the axes of the joints at points P_{i1} and P_{i2} are parallel to each other, and so are the joint axes at points P_{i3} and P_{i4}. These directions are denoted by $\mathbf{u}_{i1}$, $\mathbf{u}_{i2}$, $\mathbf{u}_{i3}$, and $\mathbf{u}_{i4}$, respectively. MEMS manufacturing processes force the link $P_{i2}P_{i3}$ to be

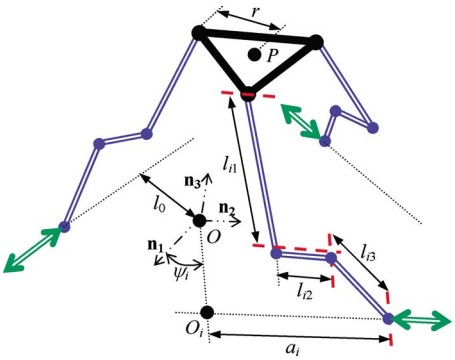

Fig. 4 Perspective view on the kinematical architecture

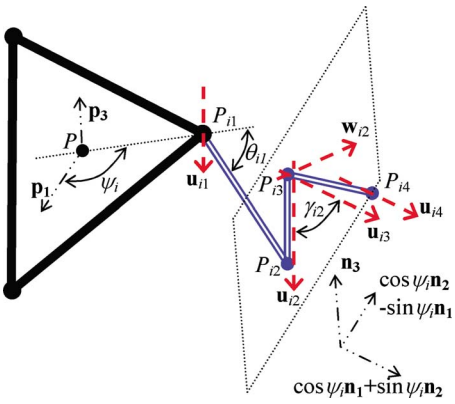

Fig. 5 The platform and one of the limbs

planar, so, without loss of generality, it can be assumed that the axes $\mathbf{u}_{i2}$ and $\mathbf{u}_{i3}$ meet at point P_{i3}. The angle between these axes is denoted by γ_{i2}.

Denote by O the origin of the coordinate system $\mathbf{n}_1$-$\mathbf{n}_2$-$\mathbf{n}_3$, located on the substrate plane, where $\mathbf{n}_3$ is perpendicular to this plane. The distances from point O to the actuators' lines of motion are indicated by l_0. The origin of the platform coordinate system, $\mathbf{p}_1$-$\mathbf{p}_2$-$\mathbf{p}_3$, is indicated by P, which is the geometric center of the equilateral triangle $P_{11}P_{21}P_{31}$. Note that this coordinate system is in general not parallel to $\mathbf{n}_1$-$\mathbf{n}_2$-$\mathbf{n}_3$, yet it maintains a fixed orientation. The distances from P to P_{i1} are denoted by r. The lengths of links $P_{i1}P_{i2}$, $P_{i2}P_{i3}$, and $P_{i3}P_{i4}$ are l_{i1}, l_{i2}, and l_{i3}, respectively. The positions of points P_{i4} are indicated by a_i and are measured from the fixed points O_i, defined as the projections of point O on the actuators' lines of motions.

3.3 Inverse Kinematics. The goal of the inverse kinematics solution is to find the positions of the actuators when the pose (position and orientation) of the moving platform is given. It should be noted that the algorithm is executed under the assumption of no joint clearance, which might be way off on the MEMS relative scale [4].

The position of the moving platform is given by a vector to its center P:

$$^{O}\mathbf{r}^{P} = x\mathbf{n}_1 + y\mathbf{n}_2 + z\mathbf{n}_3 \tag{2}$$

and the platform orientation, which is constant, is given by the orientation matrix $\mathbf{C}^P$ as

$$\begin{bmatrix}\mathbf{p}_1\\ \mathbf{p}_2\\ \mathbf{p}_3\end{bmatrix} = \begin{bmatrix}C_{11}^P & C_{12}^P & C_{13}^P\\ C_{21}^P & C_{22}^P & C_{23}^P\\ C_{31}^P & C_{32}^P & C_{33}^P\end{bmatrix} \cdot \begin{bmatrix}\mathbf{n}_1\\ \mathbf{n}_2\\ \mathbf{n}_3\end{bmatrix} \tag{3}$$

The inverse kinematics solution [20] is calculated separately for each of the three limbs ($i=1,2,3$). θ_{i1} is the pitch angle of the link $P_{i1}P_{i2}$ (Fig. 5), so that the vector from the center of the platform to P_{i3} is given as

$$\begin{aligned}^{O}\mathbf{r}^{P_{i3}} = {} & x\mathbf{n}_1 + y\mathbf{n}_2 + z\mathbf{n}_3 + (rc\psi_i + l_{i1}\cos\theta_{i1}c\psi_i - l_{i2}s\psi_i)\mathbf{p}_1\\ & + (rs\psi_i + l_{i1}\cos\theta_{i1}s\psi_i + l_{i2}c\psi_i)\mathbf{p}_2 - l_{i1}\sin\theta_{i1}\mathbf{p}_3\end{aligned} \tag{4}$$

where the angle ψ_i is constant and given as $\psi_1=0$ deg, $\psi_2=120$ deg, $\psi_3=240$ deg, and $c\psi_i=\cos\psi_i$ and $s\psi_i=\sin\psi_i$. Given that, an equation for solving θ_{i1} can be obtained:

$$^{O}\mathbf{r}^{P_{i3}} \cdot (c\psi_i\mathbf{n}_1 + s\psi_i\mathbf{n}_2) = l_0 \tag{5}$$

since P_{i3} lies in the plane indicated in Fig. 5, whose distance from O is l_0. Note that ψ_i defines also the angle of the actuator line of motion with respect to the fixed vector $\mathbf{n}_1$ (Fig. 4).

Two solutions are given by

$$\theta_{i1} = 2\tan^{-1}\left(\frac{k_{i2} \pm \sqrt{k_{i1}^2 + k_{i2}^2 - k_{i3}^2}}{k_{i3} - k_{i1}}\right) \tag{6}$$

where

$$\begin{aligned}k_{i1} &= l_{i1}[c^2\psi_i C_{11}^P + s\psi_i c\psi_i(C_{21}^P + C_{12}^P) + s^2\psi_i C_{22}^P]\\ k_{i2} &= l_{i1}[c\psi_i C_{31}^P + s\psi_i C_{32}^P]\\ k_{i3} &= r[c^2\psi_i C_{11}^P + s\psi_i c\psi_i(C_{21}^P + C_{12}^P) + s^2\psi_i C_{22}^P] + l_{i2}[c^2\psi_i C_{21}^P\\ &\quad + s\psi_i c\psi_i(C_{22}^P - C_{11}^P) - s^2\psi_i C_{12}^P] + xc\psi_i + ys\psi_i - l_0\end{aligned} \tag{7}$$

The two solutions present two assembly modes in which the link $P_{i1}P_{i2}$ is located either above the platform ($^{P_{i1}}\mathbf{r}^{P_{i2}}\cdot\mathbf{p}_3>0$), or below it ($^{P_{i1}}\mathbf{r}^{P_{i2}}\cdot\mathbf{p}_3<0$). Using Eq. (4) and the Pythagorean theorem, the travel of the actuator a_i can be found by

$$a_i = {}^{O}\mathbf{r}^{P_{i3}} \cdot (c\psi_i\mathbf{n}_2 - s\psi_i\mathbf{n}_1) \pm \sqrt{l_{i3}^2 - (^{O}\mathbf{r}^{P_{i3}} \cdot \mathbf{n}_3)^2} \tag{8}$$

Each of the actuators has two solutions; one represents an acute angle between the actuator and the adjacent link, whereas the other represents an obtuse one. Since there are less then four solutions [21], switching between these assembly modes is possible only while passing through a singular configuration in which the actuator is perpendicular to its adjacent link. Therefore, if the angles were acute at the beginning of the motion, the positive sign for the square root of Eq. (8) should be used.

We conclude that each limb has four solutions, for the two solutions of Eqs. (6) and (8). A total of 64 solutions can be found for the inverse kinematics problem of the mechanism given in Fig. 4. Indeed, this is a large number of solutions, but by applying the aforementioned algorithm to distinguish between the possible solutions, the correct solution can be easily obtained.

3.4 Design Criteria: The Angles Between the Middle Link Joints (γ_{i2}) and the Platform Orientation. The angles γ_{i2} between the joints axes of the middle link determine the platform orientation once lifted from the substrate plane. The relation between these axes is simply

$$\mathbf{u}_{i2} \cdot \mathbf{u}_{i3} = \cos\ \gamma_{i2} \tag{9}$$

where

$$\mathbf{u}_{i1} = \mathbf{u}_{i2} = s\psi_i \mathbf{p}_1 - c\psi_i \mathbf{p}_2$$
$$\mathbf{u}_{i3} = \mathbf{u}_{i4} = c\psi_i \mathbf{n}_1 + s\psi_i \mathbf{n}_2 \tag{10}$$

Using the definition of the orientation matrix given in Eq. (3) yields

$$c\gamma_{12} = -C^P_{21}$$
$$c\gamma_{22} = \frac{1}{4}[3C^P_{12} - C^P_{21} + \sqrt{3}(C^P_{22} - C^P_{11})] \tag{11}$$
$$c\gamma_{32} = \frac{1}{4}[3C^P_{12} - C^P_{21} + \sqrt{3}(C^P_{11} - C^P_{22})]$$

where $c\gamma_{ij} = \cos\ \gamma_{ij}$.

For design purposes, when the orientation matrix is known, the calculation of γ_{i2} is straightforward. On the other hand, finding the orientation matrix for a known set of angles γ_{i2} is more complicated. Applying the quaternion formula yields

$$\mathbf{C}^P = \begin{bmatrix} k_5 - k_1 & k_2 + k_3 & s_1\sqrt{2k_4 - 2k_4^2 - 2k_2k_3 + 2k_1k_5} \\ k_2 - k_3 & k_5 + k_1 & s_2\sqrt{2k_4 - 2k_4^2 + 2k_2k_3 - 2k_1k_5} \\ s_3\sqrt{2k_4 - 2k_4^2 + 2k_2k_3 + 2k_1k_5} & s_4\sqrt{2k_4 - 2k_4^2 - 2k_2k_3 - 2k_1k_5} & 1 - 2k_4 \end{bmatrix} \tag{12}$$

where

$$k_1 = (c\gamma_{22} - c\gamma_{32})/\sqrt{3}, \quad k_4 = \sqrt{k_1^2 + k_2^2}$$
$$k_2 = (c\gamma_{22} + c\gamma_{32} - 2c\gamma_{12})/3, \quad k_5 = \pm\sqrt{(k_4 - 1)^2 - k_3^2} \tag{13}$$
$$k_3 = (c\gamma_{12} + c\gamma_{22} + c\gamma_{32})/3, \quad s_1, s_2, s_3, s_4 = \pm 1$$

and the following equations are used to determine the signs of s_2, s_3, and s_4:

$$C^P_{21} = C^P_{13}C^P_{32} - C^P_{12}C^P_{33}$$
$$C^P_{22} = C^P_{11}C^P_{33} - C^P_{13}C^P_{31} \tag{14}$$
$$C^P_{23} = C^P_{12}C^P_{31} - C^P_{11}C^P_{32}$$

It follows from Eq. (13) that there are four solutions for the orientation matrix $\mathbf{C}^P$. It is worth noting that in case that the three angles γ_{i2} are equal to γ, the platform is rotated about $\mathbf{n}_3$ by $90° - \gamma$ or $90° + \gamma$, and this configuration is singular.

3.5 Full Jacobian Matrix. There might be singular configurations between the actuations and the constraint parts of the Jacobian matrix or among one of those parts [5,6]. Therefore, to detect all the singularities, the full 6×6 Jacobian matrix must be calculated. Referring to the rows of the Jacobian matrix as the governing lines of the mechanism enables an elegant way for solving the more general singularities. We refer the reader to Ref. [5], where a systematic method for forming the Jacobian matrix of limited DOF parallel mechanisms is given. The following is an implementation of Ref. [5] for our given structure.

The ith limb can resist an external torque that is applied about the direction perpendicular to its passive joints [13,19]. This direction is indicated in Fig. 5 by the unit vector $\mathbf{w}_{i2}$:

$$\mathbf{w}_{i2} = \frac{\mathbf{u}_{i2} \times \mathbf{u}_{i3}}{\sin\ \gamma_{i2}} \tag{15}$$

Hence, one screw, which is reciprocal to all the joints' screws of a limb, can be identified. This reciprocal screw, denoted as $\hat{\$}_{r,1,i}$, is an infinite pitch screw pointing in the direction of $\mathbf{w}_{i2}$:

$$\hat{\$}^T_{r,1,i} = [\mathbf{0}_{1\times 3} \quad \mathbf{w}^T_{i2}] \tag{16}$$

One additional screw, $\hat{\$}_{r,2,i}$, which is reciprocal to all the passive joint screws of the ith limb can be identified. This reciprocal screw is the intersecting line between two planes: one that contains the vectors $\mathbf{u}_{i1}$ and $\mathbf{u}_{i2}$, and one that contains $\mathbf{u}_{i3}$ and $\mathbf{u}_{i4}$ (Fig. 5). The direction of this line is

$$\mathbf{h}_i = \left(\frac{{}^{P_{i1}}\mathbf{r}^{P_{i2}}}{l_1} \times \mathbf{u}_{i2}\right) \times \left(\frac{{}^{P_{i3}}\mathbf{r}^{P_{i4}}}{l_3} \times \mathbf{u}_{i3}\right) \tag{17}$$

Since point P_{i3} lies in both planes, the intersecting line must pass through it, therefore $\hat{\$}_{r,2,i}$ is given by:

$$\hat{\$}^T_{r,2,i} = [\mathbf{h}^T_i \quad ({}^O\mathbf{r}^{P_{i3}} \times \mathbf{h}_i)^T] \tag{18}$$

This screw is a row in the Jacobian of actuations.

The full Jacobian matrix is given by

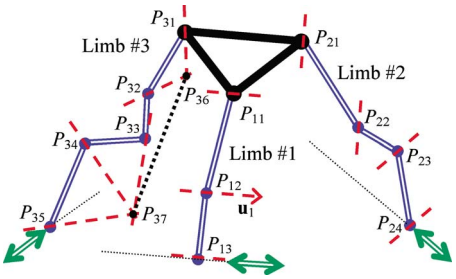

Fig. 6 Type II architecture, with three, four, and five passive joints in each limb

$$\mathbf{J} = \begin{bmatrix} & \mathbf{h}_1^T & & (^O\mathbf{r}^{P_{13}} \times \mathbf{h}_1)^T \\ & \mathbf{h}_2^T & & (^O\mathbf{r}^{P_{23}} \times \mathbf{h}_2)^T \\ & \mathbf{h}_3^T & & (^O\mathbf{r}^{P_{33}} \times \mathbf{h}_3)^T \\ 0 & 0 & 0 & \mathbf{w}_{12}^T \\ 0 & 0 & 0 & \mathbf{w}_{22}^T \\ 0 & 0 & 0 & \mathbf{w}_{32}^T \end{bmatrix} \tag{19}$$

This Jacobian matrix has similar components as it describes Type I architecture mechanisms, which consists of identical limbs. The next section deals with nontopologically identical limbs.

4 Architecture of Type II

4.1 Description. Type II architecture, which is described in Table 1, can yield a translational only mechanism, e.g., as described in Fig. 6.

The three axes of the passive joints of Limb 1 must be parallel to each other [17], so as to constrain the platform rotational movements about the two perpendicular directions. Referring to Fig. 6, the vector $\mathbf{u}_1$ denotes the direction of these joints axes. These joints allow the platform to move in a plane normal to $\mathbf{u}_1$; hence, the linear actuator has to generate motion parallel to $\mathbf{u}_1$. Limb 2 has to prevent platform rotation about $\mathbf{u}_1$. This can be achieved by arranging the four joints of Limb 2 as two pairs of parallel joints. As explained in Ref. [13], such an arrangement causes Limb 2 to constrain the platform from rotating about the direction that is perpendicular to all of its four joints. Hence, the platform is fully constrained, i.e., pure translational, if this direction is not perpendicular to $\mathbf{u}_1$, or, preferably, if it is parallel to $\mathbf{u}_1$. Limb 3 does not contribute to $\mathbf{J}_C$, and its role is to transfer the actuation forces from the base to the platform. Transferring these forces would be possible if a screw, that is reciprocal to all the limb's five passive joints, is identified. One of the possibilities to achieve this is by arranging three adjacent axes to meet at one point, while the other two axes meet at another point, so that the screw that connects these two points is, indeed, reciprocal to all five passive joints [22]. Evidently, this screw must not be perpendicular to the active joint, so they are not reciprocal to each other.

4.2 Geometric Definitions for the Suggested Architecture. Perspective skeleton views, clarifying the subsequent definitions, are shown in Figs. 6 and 7.

A platform $P_{11}P_{21}P_{31}$ is connected to the base via three limbs. Each of the limbs is connected to a linear actuator that is located on the substrate plane. Limb 1 consists of two links, whose lengths are l_{11} and l_{12}, and three joints, whose axes are parallel. Limb 2's structure is identical to that of the limbs of Type I architecture, as described in the previous section. Limb 3 consists of five revolute joints and four links, which are shown in Fig. 7. The axes of the joints are denoted by $\mathbf{u}_{3j}$ $(j=1,\ldots,5)$, and the link lengths are l_{3j} $(j=1,\ldots,4)$. The unit vector $\mathbf{v}_{3j}$ points from P_{3j} to $P_{3(j+1)}$ and, without loss of generality, is perpendicular to $\mathbf{u}_{3j}$. The unit vector $\mathbf{w}_{3j}$ is perpendicular to the link plane, where $\mathbf{w}_{3j}$

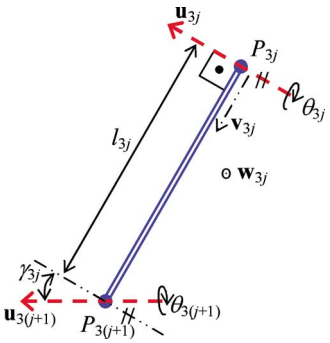

Fig. 7 Typical link of Limb 3 of Type II architecture

$=\mathbf{u}_{3j}\times\mathbf{v}_{3j}$. The constant angle between $\mathbf{u}_{3j}$ and $\mathbf{u}_{3(j+1)}$, which is determined while manufacturing, is denoted by γ_{3j}, and the changeable angle between two adjacent link planes is θ_{3j}. For simplicity, the passive joint at point P_{35} is chosen to be perpendicular to the direction of actuator motion.

In order to ensure that the axes $\mathbf{u}_{31}$ and $\mathbf{u}_{32}$ meet in one point (denoted as P_{36}), it is required that

$$\gamma_{31} \neq 0 \text{ deg} \tag{20}$$

while ensuring that the axes $\mathbf{u}_{33}$, $\mathbf{u}_{34}$, and $\mathbf{u}_{35}$ meet in one point (denoted as P_{37}) requires that

$$\frac{l_{33}}{s\gamma_{33}} = \frac{l_{34}}{t\gamma_{34}}, \quad \gamma_{33} \neq 0 \text{ deg}, \quad \gamma_{34} \neq 0 \text{ deg} \tag{21}$$

where $s\gamma_{ij}=\sin\gamma_{ij}$ and $t\gamma_{ij}=\tan\gamma_{ij}$.

4.3 Inverse Kinematics. The platform position is given in Eq. (2), while its orientation matrix is given in Eq. (3). It is worth noting that the orientation matrix is not arbitrary, since the axis $\mathbf{u}_1$ is parallel to the line of action of the corresponding actuator, meaning

$$\mathbf{u}_1 = c\psi_1\mathbf{p}_2 - s\psi_1\mathbf{p}_1 = c\psi_1\mathbf{n}_2 - s\psi_1\mathbf{n}_1 \tag{22}$$

Finding the travel of the first actuator is trivial,

$$a_1 = {}^O\mathbf{r}^{P_{11}} \cdot \mathbf{u}_1 \tag{23}$$

The algorithm for calculating the second actuator travel is identical to that of Type I mechanism limbs, which was presented in Sec. 3.3, Eqs. (4)–(8). As for the third limb, when the platform position and orientation are known, one can find the position of point P_{36}, using Eqs. (2) and (10):

$${}^O\mathbf{r}^{P_{36}} = {}^O\mathbf{r}^P + r(\cos\psi_3\mathbf{p}_1 + \sin\psi_3\mathbf{p}_2) - \frac{l_{31}}{t\gamma_{31}}\mathbf{u}_{31} \tag{24}$$

The distance from P_{37} to P_{36} is fixed and known, since both points are located at the plane of the link $P_{32}P_{33}$:

$$\left|{}^{P_{37}}\mathbf{r}^{P_{36}}\right| = \sqrt{\left(l_{32} - \frac{l_{33}s\gamma_{32}}{t\gamma_{33}}\right)^2 + \left(\frac{l_{31}}{s\gamma_{31}} - \frac{l_{33}c\gamma_{32}}{t\gamma_{33}}\right)^2} \tag{25}$$

Point P_{37} is located also at the substrate plane, in a fixed and known distance from the actuator line of action:

$${}^O\mathbf{r}^{P_{37}} = \left(l_0 - \frac{l_{34}}{s\gamma_{34}}\right)(c\psi_3\mathbf{n}_1 + s\psi_3\mathbf{n}_2) + a_3(c\psi_3\mathbf{n}_2 - s\psi_3\mathbf{n}_1) \tag{26}$$

Equating $\left|{}^{P_{37}}\mathbf{r}^{P_{36}}\right|$ from Eq. (25) to the difference between Equations (24) and (26) yields a quadratic equation in a_3, which its solutions are:

$$a_3 = k_{32} \pm \sqrt{k_{32}^2 - k_{31}} \tag{27}$$

where

$$k_{31} = |{}^{O}\mathbf{r}^{P_{36}}|^2 - |{}^{P_{37}}\mathbf{r}^{P_{36}}|^2 + \left(l_0 - \frac{l_{34}}{s\gamma_{34}}\right)^2 - 2\left(l_0 - \frac{l_{34}}{s\gamma_{34}}\right) \times (c\psi_3\, {}^{O}\mathbf{r}^{P_{36}} \cdot \mathbf{n}_1 + s\psi_3\, {}^{O}\mathbf{r}^{P_{36}} \cdot \mathbf{n}_2)$$

$$k_{32} = c\psi_3\, {}^{O}\mathbf{r}^{P_{36}} \cdot \mathbf{n}_2 - s\psi_3\, {}^{O}\mathbf{r}^{P_{36}} \cdot \mathbf{n}_1 \tag{28}$$

In order to complete the inverse kinematics solution and calculate the positions of P_{32}, P_{33}, and P_{34}, one has to find the joint angles $\theta_{31}, \ldots, \theta_{35}$. To begin with, one needs to write the following equations that relate between the coordinate systems of the platform and the upper link:

$$\begin{bmatrix} \mathbf{u}_{31} \\ \mathbf{v}_{31} \\ \mathbf{w}_{31} \end{bmatrix} = \begin{bmatrix} s\psi_3 & -c\psi_3 & 0 \\ c\psi_3 c\theta_{31} & s\psi_3 c\theta_{31} & s\theta_{31} \\ -c\psi_3 s\theta_{31} & -s\psi_3 s\theta_{31} & c\theta_{31} \end{bmatrix} \begin{bmatrix} \mathbf{p}_1 \\ \mathbf{p}_2 \\ \mathbf{p}_3 \end{bmatrix} \tag{29}$$

and, similarly, between two adjacent links:

$$\begin{bmatrix} \mathbf{u}_{3(j+1)} \\ \mathbf{v}_{3(j+1)} \\ \mathbf{w}_{3(j+1)} \end{bmatrix} = \begin{bmatrix} c\gamma_{3j} & s\gamma_{3j} & 0 \\ -s\gamma_{3j} c\theta_{3(j+1)} & c\gamma_{3j} c\theta_{3(j+1)} & s\theta_{3(j+1)} \\ s\gamma_{3j} s\theta_{3(j+1)} & -c\gamma_{3j} s\theta_{3(j+1)} & c\theta_{3(j+1)} \end{bmatrix} \times \begin{bmatrix} \mathbf{u}_{3j} \\ \mathbf{v}_{3j} \\ \mathbf{w}_{3j} \end{bmatrix} \quad (\text{for } j = 1, \ldots, 4) \tag{30}$$

where $s\theta_{ij} = \sin\theta_{ij}$ and $c\theta_{ij} = \cos\theta_{ij}$.

Observing Fig. 6 yields

$${}^{O}\mathbf{r}^{P_{37}} = {}^{O}\mathbf{r}^{P_{31}} + l_{31}\mathbf{v}_{31} + l_{32}\mathbf{v}_{32} - \frac{l_{33}}{t\gamma_{33}}\mathbf{u}_{33} \tag{31}$$

where ${}^{O}\mathbf{r}^{P_{37}}$ is already known from Eqs. (26) and (27). Scalar multiplication of Eq. (31) by $\mathbf{u}_{31}$ and using of Eq. (30) enable solving the angle θ_{32}:

$$\theta_{32} = \pm \cos^{-1}\left(\frac{({}^{O}\mathbf{r}^{P_{37}} - {}^{O}\mathbf{r}^{P_{31}}) \cdot \mathbf{u}_{31} t\gamma_{33} + l_{33} c\gamma_{31} c\gamma_{32}}{(l_{33} s\gamma_{32} - l_{32} t\gamma_{33}) s\gamma_{31}}\right) \tag{32}$$

Other scalar multiplications of Eq. (31), by $\mathbf{p}_1$ and $\mathbf{p}_3$, yield the following equations:

$$\begin{bmatrix} \cos\theta_{31} \\ \sin\theta_{31} \end{bmatrix} = \begin{bmatrix} k_{33} c\psi_3 & -k_{34} c\psi_3 \\ k_{34} & k_{33} \end{bmatrix}^{-1} \cdot \begin{bmatrix} k_{35} \\ k_{36} \end{bmatrix} \tag{33}$$

where

$$k_{33} = l_{31} t\gamma_{33} + c\gamma_{31} c\theta_{32} (l_{32} t\gamma_{33} - l_{33} s\gamma_{32}) - l_{33} c\gamma_{32} s\gamma_{31}$$

$$k_{34} = s\theta_{32} (l_{32} t\gamma_{33} - l_{33} s\gamma_{32})$$

$$k_{35} = ({}^{O}\mathbf{r}^{P_{37}} - {}^{O}\mathbf{r}^{P_{31}}) \cdot \mathbf{p}_1 t\gamma_{33} + [s\gamma_{31} c\theta_{32} (l_{32} t\gamma_{33} - l_{33} s\gamma_{32}) + l_{33} c\gamma_{32} c\gamma_{31}] s\psi_3$$

$$k_{36} = ({}^{O}\mathbf{r}^{P_{37}} - {}^{O}\mathbf{r}^{P_{31}}) \cdot \mathbf{p}_3 t\gamma_{33} \tag{34}$$

Solving both rows of Eq. (33) yields a unique value for θ_{31}. Now it is possible, using Eqs. (29) and (30), to calculate the vectors $\mathbf{u}_{32}$ and $\mathbf{v}_{32}$.

Similarly, one can solve also the angle θ_{34}:

$$\theta_{34} = \pm \cos^{-1}\left(\frac{c\gamma_{34} c\gamma_{33} - (c\psi_3 \mathbf{n}_1 + s\psi_3 \mathbf{n}_2) \cdot (c\gamma_{32} \mathbf{u}_{32} + s\gamma_{32} \mathbf{v}_{32})}{s\gamma_{33} s\gamma_{34}}\right) \tag{35}$$

and then the angles θ_{33} and θ_{35}:

$$\begin{bmatrix} \cos\theta_{33} \\ \sin\theta_{33} \end{bmatrix} = \begin{bmatrix} k_{37} & -k_{38} \\ k_{38} & k_{37} \end{bmatrix}^{-1} \cdot \begin{bmatrix} k_{39} \\ k_{40} \end{bmatrix}$$

$$\begin{bmatrix} \cos\theta_{35} \\ \sin\theta_{35} \end{bmatrix} = \begin{bmatrix} k_{41} & -k_{42} \\ k_{42} & k_{41} \end{bmatrix}^{-1} \cdot \begin{bmatrix} k_{43} \\ k_{44} \end{bmatrix} \tag{36}$$

where

$$k_{37} = c\gamma_{34} s\gamma_{33} + s\gamma_{34} c\gamma_{33} c\theta_{34}, \quad k_{41} = s\gamma_{34} c\gamma_{33} + c\gamma_{34} s\gamma_{33} c\theta_{34}$$

$$k_{38} = s\gamma_{34} s\theta_{34}, \quad k_{42} = s\gamma_{33} s\theta_{34}$$

$$k_{39} = (c\psi_3 \mathbf{n}_1 + s\psi_3 \mathbf{n}_2) \cdot (-s\gamma_{32} \mathbf{u}_{32} + c\gamma_{32} \mathbf{v}_{32})$$

$$k_{43} = (s\psi_3 \mathbf{n}_1 - c\psi_3 \mathbf{n}_2) \cdot (c\gamma_{32} \mathbf{u}_{32} + s\gamma_{32} \mathbf{v}_{32}) \tag{37}$$

$$k_{40} = (c\psi_3 \mathbf{n}_1 + s\psi_3 \mathbf{n}_2) \cdot \mathbf{w}_{32}, \quad k_{44} = \mathbf{n}_3 \cdot (c\gamma_{32} \mathbf{u}_{32} + s\gamma_{32} \mathbf{v}_{32})$$

Hence, the third limb can have eight solutions, as there are two postures in each of Eqs. (27), (32), and (35). The first limb has two solutions (elbow up/down), and four solutions can be obtained for the second limb. A total of 64 solutions can be found to the inverse kinematics problem, exactly the same number as the symmetric architecture of Type I.

4.4 Full Jacobian Matrix. The Jacobian of actuations consists of three screws, which are reciprocal to all the passive joints, one row for each limb:

$$\mathbf{J}_A = \begin{bmatrix} \mathbf{u}_1^T & ({}^{O}\mathbf{r}^{P_{13}} \times \mathbf{u}_1)^T \\ \mathbf{h}_2^T & ({}^{O}\mathbf{r}^{P_{23}} \times \mathbf{h}_2)^T \\ \left(\frac{{}^{P_{37}}\mathbf{r}^{P_{36}}}{|{}^{P_{37}}\mathbf{r}^{P_{36}}|}\right)^T & \left({}^{O}\mathbf{r}^{P_{37}} \times \frac{{}^{P_{37}}\mathbf{r}^{P_{36}}}{|{}^{P_{37}}\mathbf{r}^{P_{36}}|}\right)^T \end{bmatrix} \tag{38}$$

where $\mathbf{u}_1$, $\mathbf{h}_2$, and $|{}^{P_{37}}\mathbf{r}^{P_{36}}|$ were taken from Eqs. (22), (17), and (25), respectively.

The Jacobian of constraints consists of three directions that the platform cannot rotate about—two that are perpendicular to the first limb axes, and one that is perpendicular to the axes of the second limb, as described in Eq. (15):

$$\mathbf{J}_C = \begin{bmatrix} \mathbf{0}_{1\times 3} & \mathbf{n}_3^T \\ \mathbf{0}_{1\times 3} & c\psi_1 \mathbf{n}_1^T + s\psi_1 \mathbf{n}_2^T \\ \mathbf{0}_{1\times 3} & \mathbf{w}_{22}^T \end{bmatrix} \tag{39}$$

5 Numerical Examples

5.1 Type I Architecture. Suppose that the angles between the joints' axes of the middle link (Fig. 2) are $\gamma_{12}=60$ deg, $\gamma_{22}=90$ deg, and $\gamma_{32}=120$ deg. Substituting these values in Eq. (13) yields $k_1=0.2887$, $k_2=-0.5$, $k_3=0$, $k_4=0.5774$, and $k_5=0.4226$, for positive k_5. Choosing $s_1=1$ in Eq. (12) yields the following orientation matrix:

$$\mathbf{C}^P = \begin{bmatrix} 0.1340 & -0.5000 & 0.8556 \\ -0.5000 & 0.7113 & 0.4940 \\ -0.8556 & -0.4940 & -0.1547 \end{bmatrix} \tag{40}$$

The platform radius is taken as $r=120$, and the distances to the lines of action of the actuators are $l_0=300$. The link lengths are $l_{i1}=350$, $l_{i2}=100$, and $l_{i3}=400$, for the three limbs ($i=1,2,3$). Assume that ${}^{O}\mathbf{r}^{P} = 100\mathbf{n}_1 + 350\mathbf{n}_3$ is the required platform location. The angles θ_{i1} can be found using Eq. (6): $\theta_{11}=120.6$ deg, $\theta_{21}=48.9$ deg, and $\theta_{31}=-60.6$ deg. Note that Eq. (6) yields two solutions, and the acceptable ones are the maximal values of θ_{i1}, where the link $P_{i1}P_{i2}$ is located below the platform. For these values, the locations of the actuators are calculated using Eq. (8) as $a_1=303.38$, $a_2=-89.35$, and $a_3=539.62$. Now, by using Eqs. (17) and (19), the full Jacobian matrix is obtained:

$$\mathbf{J} = \begin{bmatrix} -0.8320 & -0.0748 & 0.5456 & 165.53 & -493.41 & 184.74 \\ 0.1872 & 0.7061 & 0.5503 & 36.58 & -35.66 & 33.31 \\ 0.1597 & 0.8628 & 0.0778 & -114.65 & 17.75 & 38.62 \\ 0 & 0 & 0 & 0 & -0.5704 & 0.8214 \\ 0 & 0 & 0 & -0.8556 & -0.4940 & -0.1547 \\ 0 & 0 & 0 & -0.4940 & 0.2852 & 0.8214 \end{bmatrix} \tag{41}$$

The Jacobian matrix consists of the governing lines of the mechanism, and the linear complex that is closest to these lines [23] is $[0\ 0\ 0\ -0.5702\ 0.4168\ -0.7079]$. The pitch of this linear complex is infinite, meaning that the instantaneous motion of the platform is indeed translational, and the mechanism is not singular.

5.2 Type II Architecture. To withstand the condition in Eq. (22), assume that the platform inclines by 40 deg about $\mathbf{n}_2$, so the orientation matrix is

$$\mathbf{C}^P = \begin{bmatrix} 0.7660 & 0 & -0.6428 \\ 0 & 1 & 0 \\ 0.6428 & 0 & 0.7660 \end{bmatrix} \tag{42}$$

Let the platform location and the lengths of the second limb's links be same as in the previous example. The third limb's link lengths are taken as $l_{31}=180$, $l_{32}=140$, $l_{33}=200$, and $l_{34}=145.09$, so Eq. (21) is obeyed.

Substituting in Eqs. (23) and (8) gives the actuators travels $a_1=0$ and $a_2=451.53$. Substituting in Eq. (17) yields $\mathbf{h}_2=0.7989\mathbf{n}_1-0.3009\mathbf{n}_2+0.4450\mathbf{n}_3$. As for the third limb, Eq. (25) yields the distance $|{}^{P_{37}}\mathbf{r}^{P_{36}}|=360.36$, and Eq. (27) yields two solutions for the actuator travel: $a_3=82.48$ or $a_3=538.96$. For the first solution, the difference between Eqs. (24) and (26) is ${}^{P_{37}}\mathbf{r}^{P_{36}}=131.49\mathbf{n}_1-228.72\mathbf{n}_2+245.47\mathbf{n}_3$. The joint angles are calculated using Eqs. (32)–(37): $\theta_{31}=-71.63$ deg, $\theta_{32}=-68.90$ deg, $\theta_{33}=128.71$ deg, $\theta_{34}=-65.76$ deg, and $\theta_{35}=103.26$ deg, where the negative values were chosen for θ_{32} and θ_{34}, arbitrarily. The third limb contributes one row to the Jacobian matrix, which can be found using Eqs. (38) and (39):

$$\mathbf{J} = \begin{bmatrix} 0 & 1 & 0 & 0 & 0 & 300 \\ 0.7989 & -0.3009 & 0.4450 & 160.323 & 324.558 & -68.361 \\ 0.3649 & -0.6347 & 0.6812 & -2.5425 & -63.407 & -57.720 \\ 0 & 0 & 0 & 0 & 0 & 1 \\ 0 & 0 & 0 & 1 & 0 & 0 \\ 0 & 0 & 0 & 0.4846 & 0.2798 & 0.8288 \end{bmatrix} \tag{43}$$

The linear complex is $[0\ 0\ 0\ 0.6240\ -0.1030\ -0.7745]$, and its pitch is infinite, as expected.

6 Summary and Conclusions

Two architectures of translational parallel mechanisms that comply with MEMS fabrication limitations were suggested. The mechanisms are comprised of three linear actuators and 12 revolute joints that are fabricated within the substrate plane. Only a few combinations of joint arrangements are possible, if pure translational motion is desired. The kinematical requirements include, among others, the avoidance of constraint singularities that are associated with limited DOF parallel mechanisms. All the singularities were found by examining the full Jacobian matrix, which was calculated by identifying the governing lines of the mechanism. It was shown that these architectures are indeed functional, despite the severe limitations forced by current MEMS fabrication techniques. These limitations may be changed when new micromanufacturing technologies are introduced, and consequently, increase the number of feasible architectures.

A methodical approach for designing architectures of translational microparallel mechanisms was developed. The approach is denoted as MEMS kinematics, where both MEMS fabrication limitations and kinematical considerations were taken into consideration.

Realization of the present microrobot still faces some major obstacles: hinge reliability, during fabrication and operation, can cause low yield, especially due to the large number of hinges included in the mechanism. Raising the device from its planar fabrication pose is also a challenge. Clearances at the joints can reduce the positional accuracy of the moving platform to a degree that it is not useable, as was discussed in a previous investigation [4]. These obstacles are a challenge in all currently realized micromechanisms and are subjects for further investigation.

References

[1] Pister, K. S. J., Judy, M. W., Burgett, S. R., and Fearing, R. S., 1992, "Micro-Fabricated Hinges," Sens. Actuators, A, **33**(3), pp. 249–256.

[2] Fan, L., Wu, M. C., Choquette, K. D., and Crawford, M. H., 1997, "Self-Assembled Microactuated XYZ Stages for Optical Scanning and Alignment," *Proceedings of International Solid State Sensors and Actuators Conference (Transducers'97)*, Chicago, IL, pp. 319–322.

[3] Chablat, D., and Wenger, P., 2003, "Architecture Optimization of a 3-DOF Translational Parallel Mechanism for Machining Applications, the Orthoglide," IEEE Trans. Rob. Autom., **19**(3), pp. 403–410.

[4] Bamberger, H., Shoham, M., and Wolf, A., 2006, "Kinematics of Micro Planar Parallel Robot Comprising Large Joint Clearances," *Advances in Robot Kinematics (ARK)*, Springer, Ljubljana, Slovenia, pp. 75–84.

[5] Joshi, S. A., and Tsai, L.-W., 2002, "Jacobian Analysis of Limited-DOF Parallel Manipulators," ASME J. Mech. Des., **124**, pp. 254–258.

[6] Zlatanov, D., Bonev, I. A., and Gosselin, C. M., 2002, "Constraint Singularities of Parallel Mechanisms," *IEEE International Conference on Robotics and Automation (ICRA)*, Washington, DC, pp. 496–502.

[7] Kim, D., and Chung, W. K., 2003, "Kinematic Condition Analysis of Three-DOF Pure Translational Parallel Manipulators," ASME J. Mech. Des., **125**, pp. 323–331.

[8] Hao, F., and McCarthy, J. M., 1998, "Conditions for Line-Based Singularities in Spatial Platform Manipulators," J. Rob. Syst., **15**(1), pp. 43–55.

[9] Fang, Y., and Tsai, L.-W., 2004, "Structure Synthesis of a Class of 3-DOF Rotational Parallel Manipulators," IEEE Trans. Rob. Autom., **20**(1), pp. 117–121.

[10] Zoppi, M., Bruzzone, L. E., Molfino, R. M., and Michelini, R. C., 2003, "Constraint Singularities of Force Transmission in Nonredundant Parallel Robots With Less Than Six Degrees of Freedom," ASME J. Mech. Des., **125**, pp. 557–563.

[11] Gosselin, C., and Angeles, J., 1990, "Singularity Analysis of Closed-Loop Kinematic Chains," IEEE Trans. Rob. Autom., **6**(3), pp. 281–290.

[12] Zlatanov, D., Fenton, R. G., and Benhabib, B., 1998, "Identification and Classification of the Singular Configurations of Mechanisms," Mech. Mach. Theory, **33**(6), pp. 743–760.

[13] Carricato, M., and Parenti-Castelli, V., 2003, "A Family of 3-DOF Translational Parallel Manipulators," ASME J. Mech. Des., **125**, pp. 302–307.

[14] Grübler, M., 1917, *Getriebelehre*, Springer-Verlag, Berlin.

[15] Rico Martinez, J. M., and Ravani, B., 2003, "On Mobility Analysis of Linkages using Group Theory," ASME J. Mech. Des., **125**, pp. 70–80.

[16] Gogu, G., 2005, "Mobility of Mechanisms: A Critical Review," Mech. Mach. Theory, **40**(9), pp. 1068–1097.

[17] Carricato, M., and Parenti-Castelli, V., 2004, "On the Topological and Geometrical Synthesis and Classification of Translational Parallel Mechanisms," *Proceedings of the 11th World Congress in Mechanisms and Machine Science*, Tianjin, China.

[18] Bamberger, H., and Shoham, M., 2004, "Kinematic Structure of a Parallel Robot for MEMS Fabrication," *On Advances in Robot Kinematics (ARK)*,

Kluwer Academic, Sestri-Levante, Italy, pp. 113–122.
[19] Bamberger, H., Wolf, A., and Shoham, M., 2005, "Identification of Micro Parallel Robot's Singularity Using Line Geometry," *The 30th Israeli Conference on Mechanical Engineering*, Tel-Aviv, Israel.
[20] Carricato, M., and Parenti-Castelli, V., 2003, "Position Analysis of a New Family of 3-DOF Translational Parallel Manipulators," ASME J. Mech. Des., **125**, pp. 316–322.
[21] Innocenti, C., and Parenti-Castelli, V., March 1998, "Singularity-Free Evolution from One Configuration to Another in Serial and Fully-Parallel Manipulators," ASME J. Mech. Des., **120**, pp. 73–79.
[22] Di-Gregorio, R., and Parenti-Castelli, V., 2006, "Parallel Mechanisms for Knee Orthoses with Selective Recovery Action," *On Advances in Robot Kinematics (ARK)*, Kluwer Academic, Ljubljana, Slovenia, pp. 167–176.
[23] Wolf, A., and Shoham, M., 2003, "Investigation of Parallel Manipulators Using Linear Complex Approximation," ASME J. Mech. Des., **125**(3), pp. 564–572.